STEADY OPERATION OF AN ELECTROMAGNETIC PLASMOID THRUSTER

David Kirtley, John Slough, Michael Pfaff, and Chris Pihl
MSNW LLC, Redmond, WA.

ABSTRACT

The Electromagnetic Plasmoid Thruster (EMPT) is an electric propulsion thruster and power processing system that will allow a dramatic decrease in system mass and increase lifetime over traditional 500-5000 W propulsion systems. The EMPT employs a Rotating Magnetic Field (RMF) to produce large plasma currents inside a conical thruster creating a field-reversed (FRC) plasmoid that is magnetically isolated from the thruster walls. The intensified gradient magnetic field from the plasmoid, together with the large plasma currents, result in a large body force which expels the plasmoid at high velocity. The EMPT is a pulsed device, nominally operating at 1 kW with 1 Joule discharges. Presented is a theoretical introduction to the EMPT and current experimental results with operation from 500-5000 Watts. First, FRC formation and translation has been demonstrated at a scale not seen before, both in energy and in physical size. The EMPT has demonstrated that it is possible to build high-efficiency pulsed-inductive devices in the 1 J and 1 kW class of pulsed thruster. Finally, the EMPT has demonstrated multi-pulse and steady state operating of a pulsed-inductive-type thruster. Experimental results as well as thermal, engineering, and plasma design considerations for a steady operating pulsed thruster will be discussed. This paper seeks to provide an initial framework for considering the design and steady operation of pulsed, gaseous electromagnetic thrusters. Gas utilization and input circuit energy efficiencies will be described. Single pulse and steady operation results of a 1 kW thruster will be presented. And finally, an overview of thermal modeling, thermal engineering considerations, and long-life thruster design will be presented.

DESIGN CONSIDERATIONS FOR STEADY OPERATION OF A PULSED PLASMA THRUSTER

Gas Utilization in High-Density, Magnetized FRC Thrusters

Pulsed plasma thrusters have been developed in a wide variety of types and propellants from solid propellant arc discharge thrusters to gaseous pulse inductive thrusters. Pulsed thrusters have numerous performance and operational benefits, including highly throttleable power, increased power density, and precision impulse-bit operation. However, they also have numerous, sometimes unpredicted challenges transitioning from a single pulse operation to steady operation.

A primary issue for gas fed pulse plasma thrusters, including gaseous fed pulse inductive thrusters, is the gas handling system and utilization. A typical gaseous fed pulse thruster uses a high speed puff valve, in which has serious lifetimes concerns; additionally, it has been found by MSNW and others [1, 2], that even the highest speed valve (and in this case the authors are referring to less than 80 microseconds opening time), the realities of a gas injection system and a thruster-like configuration yield many milliseconds of gas flow per puff within the thruster body. This inevitably leads to gas on the forefront and the trailing edge of the gas puff that is of an undesired magnitude and location. This extra propellant is either not used by the plasma discharge or is utilized in a non-optimal manner. Therefore, it is the authors' beliefs that a pulsed plasma system of any kind must be operated in a burst mode in which a single gas puff of ten or more milliseconds is used to supply propellant for many electrical and thruster discharges. In this way it is believed that the effects of lead and trailing edge gases can be highly mitigated. For a long duration spacecraft mission that requires long periods of continuous operation, puff valves become a life-limiting concern in their entirety. In these cases it is clearly desirable to operate with a steady operating gas flow and a pulsed electrical system. Additionally, for lower power thrusters such

as the 1 kW systems described here, bursts of minutes and hours can be realized with small battery systems.

In addition to the total gas/propellant utilization before and after firing, the utilization of a gas during a single discharge is critical to proper and efficient operation. Gas utilization during a discharge has been looked at extensively in FRC thrusters and FRC-based fusion devices [3]. It has been found that the high plasma density and general inward radial plasma flow due to compressing fields and rotating magnetic fields lends FRC thrusters to very high gas utilization efficiency. Current thruster testing work will validate the single-pulse empirical studies that have been done previously in a more traditional manner on a thrust stand with steady flowing gas. However, several key experiments involving the multi-pulse EMPT can be leveraged in order to form a robust conclusion of gas utilization in these high density plasma thrusters with only a single pulse. Several key gas utilization conclusions that separate FRC-based devices from other pulsed plasma thrusters include:

- With few exceptions, the downstream probe density measurements are within 50% of the expected plasma density from measured neutral gas flow and single-shot thrust measurements. This is well within the error range for a double Langmuir probe in a flowing, supersonic plasma.
- For the multi-pulse EMPT testing it was found that after the magnetic signature of the FRC had translated out of the device (from external probes) there was no evidence of diamagnetism or inductive loading. This suggests that there was little or no gas left in the device to form a plasma. As will be described later, the key requirement for steady operating of the EMPT was allowing sufficient neutral gas refill time between discharges. The expected neutral refill time of the EMPT is 280-560 μs depending on the neutral flow velocity.
- In large-scale fusion DOE experiments, it is clear that FRC plasma sweep up all background gases and compress it. This has been shown in contamination studies [4].
- It is expected that an FRC would sweep up most of the propellant in the device. The ion-neutral collision mean free path is 3-10 mm, leading to significant interaction of the radially and axial plasma population with background neutrals.

In the following experimental discussion the results of initial steady operation testing will describe the results from multi-pulse operation of an electromagnetic thruster, with a particular focus on gas utilization.

Multi-Pulse Circuit Energy Utilization and Pulse Charging

In addition to propellant utilization, the other major concerns for pulsed plasma thrusters involve circuit and energy utilization. A continuously operating pulsed plasma system discharges at a typical duty cycle of 500 to 5000 Hz, depending on the geometry and propellant used in that particular thruster. For the thrusters to be described later, the optimal duty cycle is 2800 Hz for a 1-5 kilowatt thruster operating on Xenon. The maximum repetition rate is set by the neutral refill time of the thruster. A minimum repetition rate is set by the gas utilization as described earlier, as well as the pre-ionization requirement for shot to shot repeatability. For these devices it is critical that either energy is completely drained from this capacitor and used in the plasma discharge, or the remaining energy is absorbed back into the energy storage system through inductive energy recovery to be reused on subsequent firings. For the FRC thrusters that will be described subsequently, it has been found that they are very energy efficient. They have demonstrated coupling of greater than 90% with energy from the capacitor being transferred into the plasma as either internal or kinetic energy. Other detailed efforts have looked at energy coupling efficiencies for single-shot pulse inductive thrusters, as well as electrode plasma thrusters [5, 6].

A unique topic however, is the circuit requirements for a steady operating pulsed electromagnetic thruster. In a pulsed thruster the average power is determined by the repetition rate of the thruster operation. In the systems described here, typical duty cycles are 1-20%. This results in several interesting phenomena that are critical to pulsed circuit design. First, the instantaneous power is several orders of magnitude higher than the average power. For EMPT tested here, a 5.6 kW average power operation was the result of 2800 Hz operation of 2 Joules, a peak power of 17 MW (peak voltage times peak current), and an operating power of 35 kW (average power divide by duty cycle). These vastly disparate power levels lead to interesting circuit design challenges. Additionally, they are the source of a pulsed thruster's performance advantages, in that as the operational power increases, the ratio of kinetic energy to plasma formation and frozen flow energies dramatically increases, so each individual discharge can be highly efficient. The key is designing a circuit system which can handle the large peak powers, but is also lightweight and efficient for operation at low average (and spacecraft operating) powers.

THRUSTER DESCRIPTION

Background- RMF and FRC propulsion

A field reversed configuration (FRC) plasma consists of a closed field line, fully magnetized plasma with a large azimthal current (as in Figure 1). The plasma diamagnetic current is generated opposite to the applied external field, creating a high-pressure configuration [7]. Typical FRC plasmas are formed with fast (10's of μs), large (10's of kA) inductive discharges.

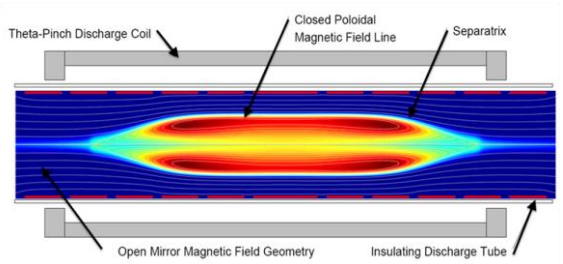

Figure 1. Cross section of a cylindrical field reversed configuration plasma

The generation of FRCs using rotating magnetic fields (RMF) is well established [8]. The transverse rotating magnetic field is produced by external antennas as indicated in Figure 2. The first pair of loop antennas, carrying a sinusoidally occillating current, produce a uniform magnetic field transverse to the coil axis as shown in black. A second loop pair produce a transverse magnetic field perpendicular to the first pair (blue) and are driven 90° out of phase with respect to the first pair. The composite magnetic field then forms a rotating, transverse magnetic field of constant magnitude. An electron magnetized to the field lines will rotate azimuthally on average at the same frequency as the antennas. An axial bias field is applied and, if the magnetude of the RMF induced J_θ is suffient to reverse this field, a true field reversed plasma is formed as in Figure 3. For an axially-distributed RMF system it is found that the azimuthal current is quite simply:

$$J_\theta = en_e\omega r$$

The EMPT thruster forms a RMF in a conical, gradient magnetic bias field as shown in Figure 4. The large J_θ is driven in a conical field with a radial magnetic field. The fully-formed FRC is then accelerated axially by the resultant $J_\theta xB_r$ force. The azimuthal current continues to be generated as the FRC moves downstream and the FRC accelerates throughout the entire

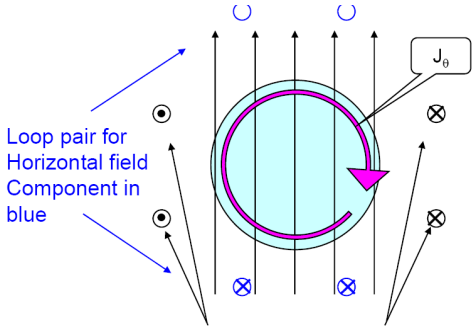

Figure 2. Schematic of an RMF

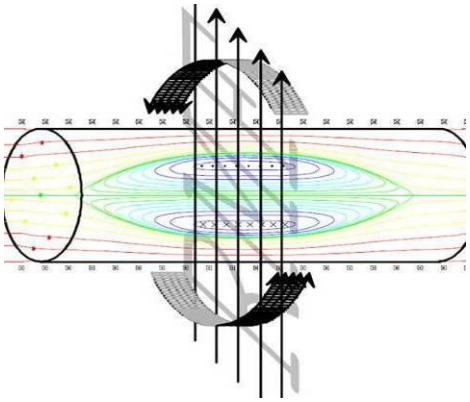

Figure 3. Schematic of a Rotating Magnetic Field creating an FRC

cone. Finally, as the FRC expands through the conical section and beyond the exit of the cone, the thermal energy of the FRC is converted into axial velocity as in a typical magnetic expansion, resulting in a low temperature, high velocity compact plume. This entire process, the underlying physics, transition to FRC, and the ejection process have been detailed in several earlier publications [9, 10].

EMPT Thruster

The EMPT program seeks to characterize the steady state performance of a 1 kW class RMF-formed Xenon FRC thruster. The EMPT has demonstrated the single and multi-pulse operation of FRC thrusters and radically advanced the field of pulse inductive thruster technology. The EMPT has demonstrated several important firsts:

- The first formation of a pulsed-inductive plasma at <1 Joule per pulse
- Demonstrated formation and ejection of a Xenon FRC at the equivalent of 500-7,000 s Isp
- Formed, ejected, and measured downstream travel of 1-50 Xenon plasmoids at 2,800 Hz
- Designed, tested, and fully integrated a lightweight inductive pulse charging circuit that uses a 250 V bus voltage to drive a 1,300 V discharge circuit
- Proved multiple FRC formation with a single pre-ionization, realizing a thruster with 300,000 restarts
- Operated multiple FRC discharges with a steady-state gas flow

This paper has discussed pulsed electromagnetic, pulsed inductive, FRC, and RMF-formed FRC thrusters, all in order of increases specificity. FRC thrusters are pulsed inductive thrusters in which the plasma has significant thermal energy and magnetic pressure. Additionally, there must be trapped magnetic flux such that the magnetized plasma forms a radial equilibrium with an applied external field [9]. RMF-formed FRC thrusters are an extension of these advanced of theta-pinch-formed-FRC thrusters in which the large plasma current is inducted with a rotating field, rather than azimuthal induction.

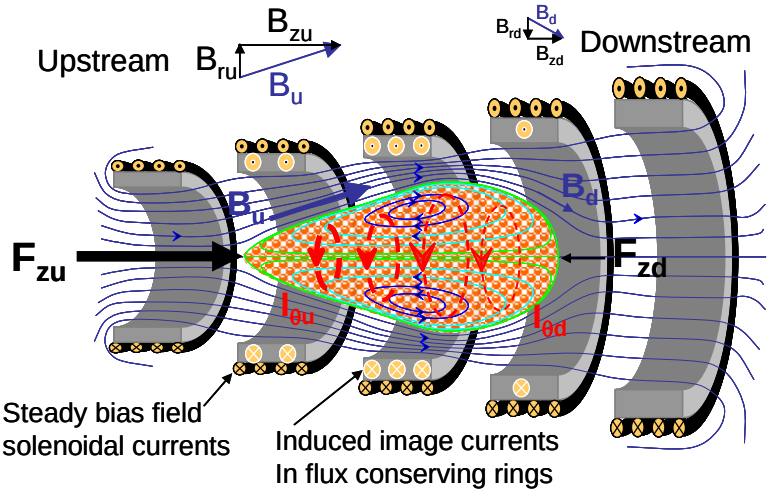

Figure 4. Schematic of the basic elements of EMPT operation. In the setting of a conical thruster configuration the upstream axial Lorentz force ($I_{\theta u} \times B_{ru}$) on FRC much larger than downstream force pushing back ($I_{\theta d} \times B_{rd}$) as both the FRC current I_θ and conical field fall off as $1/r^2$. Radial confining force ($I_\theta \times B_z$) confines FRC away from wall at all times but drops with FRC I_θ and coil B_z so that FRC expands and cools converting thermal to directed energy.

Multi-Pulse Circuit Design

The discharge circuit for EMPT has been designed and tested using several RF and pulsed power techniques developed at MSNW as well as incorporating new, advanced generation solid-state switches. The EMPT plasma discharges described below utilized the version 1 discharge circuit shown in Figure 5. The EMPT v1 was operated with 8 conservative (4 kV-rated) high-Q poly-foil capacitors per antenna with

less than 1 mOhm total resistance and two 9 kA-capable high-speed Semikron IGBT switches as shown in Figure 5. While not optimal performance, these version 1 circuit choices were a good balance of cost, performance, and de-rating. Current testing and circuits shown in the later discussion on steady thermal operation utilize smaller, higher efficiency IGBT switches operated in parallel and very high-Q, high-temperature, ceramic capacitors. The discharge circuit is a simple L-C ringing oscillator in which the high power capacitors are pulse charged to the thruster operating voltage (500-1000 Volts) and are switched by the solid-state switches. The underdamped oscillating circuit discharges and transfers energy to the plasma, generating a rotating magnetic field, and accelerating the plasma.

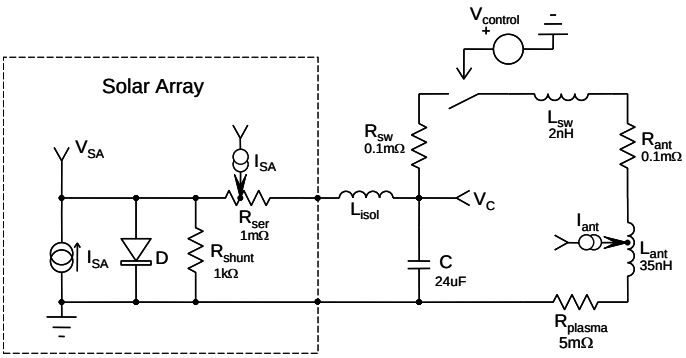

Figure 6. Circuit schematic for EMPT PPU and constant current solar array source.

Each capacitor-switch pair drives an individual Litz wire bundle of 2000, 44-AWG, insulated wires that are operated in parallel to form a single, high-Q LC oscillator for RMF generation. The discharge time for EMPT is roughly 50 μsec, with the remaining time between pulses used for Xenon gas refilling and capacitor recharging. Past research has exclusively used high-voltage power supplies to charge a capacitor bank or energy storage network. This technique requires heavy, temperature sensitive, radiation sensitive and very expensive DC-DC transformers. Therefore MSNW uses an innovative technology, active pulsed inductive charging, to dramatically decrease PPU and spacecraft bus requirements.

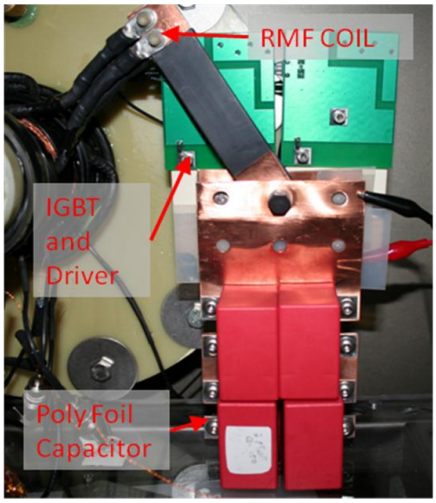

Figure 5. Photograph of the EMPT discharge circuit. Shown are RMF Coil B, 8 poly foil high-Q capacitors, and parallel high-current IGBTs. Also shown are key strip-line feeds and Litz antenna.

In this inductive pulsed charging circuit a 200 μH choke inductor stores magnetic energy between discharges. This choke inductor then recharges the fast capacitors to a much higher voltage than the bus charging voltage. The resulting charge voltage is determined by the inductance and capacitance values used. In the experiments at MSNW LLC, the pulse charging system routinely takes a DC charging voltage of 24 Volts and very efficiently increases the available voltage up to 1200 Volts on the RMF capacitors. A small charging current is needed to complete the charging cycle. Figure 6 shows the preliminary discharge circuit, while Figure 7 shows spice modeling results. Finally, a small, low voltage capacitor can be used to stabilize current draw from the spacecraft battery systems to less than 5% current draw ripple. Two of the most significant characteristics of this system are that the additional hardware required to modify charge voltage is passive and easily capable of high-temperature operation and that the final charge voltage, average power, and space-craft current draw can be modified by the switching time of the primary discharge switching. And while this makes the pulsed power switching the critical thermal and lifetime limiting component, it removes the need for a large number of extra radiation and thermally sensitive hardware. These systems will be further described in the thermal modeling discussion later in this paper.

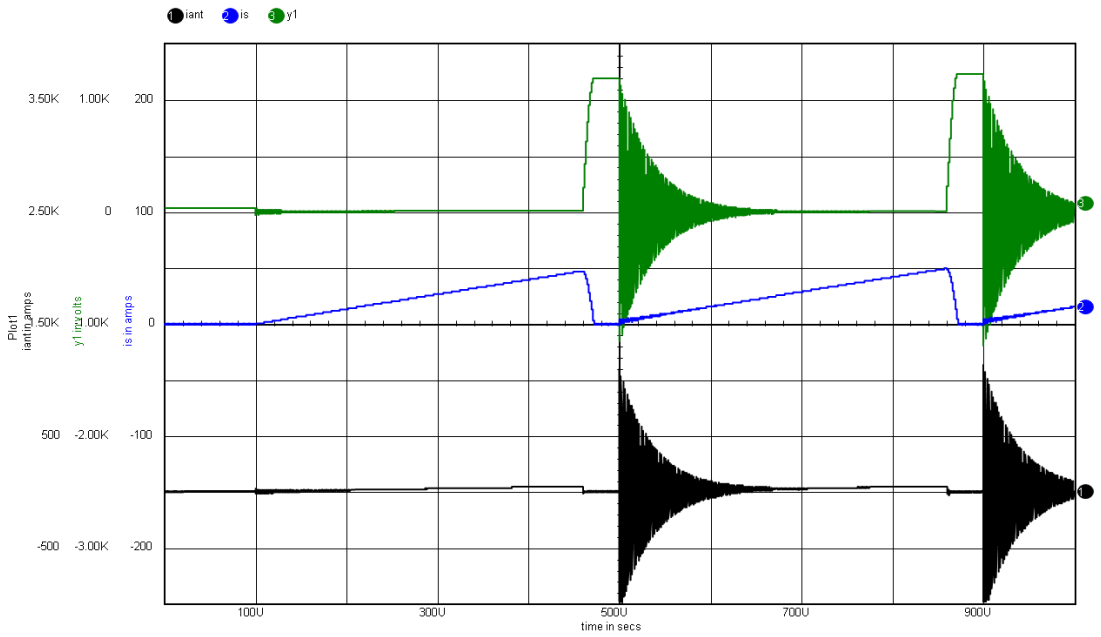

Figure 7. Circuit results. Shown is a 2 kHz discharge frequency with a 300 kHz RF frequency. Shown in green is capacitor voltage, blue is battery draw, black is antenna current.

Thruster Hardware Design

The Electromagnetic Plasmoid Thruster has a thin (3 mm) conical quartz insulator that forms the primary thruster structure, electrical insulation, and neutral gas containment. Three EMPT versions have been constructed to date, though data in this paper is limited to the first iteration. Each thruster uses a conical quartz insulator. EMPT v1 was 10 degrees, while later versions are 12 degrees. Bias field magnets and magnetic flux conserver/shapers are located directly on the insulator. Litz wire RMF antennas are attached to the thruster body to the bias field magnets. EMPT versions 2 and 3 include higher efficiency bias field magnets, lightweight aluminum flux conservers, further decreases in thruster geometry, and integration of thermal concerns. Figure 8 shows a labeled cross section of the thruster, Figure 9 shows the EMPT v1 attached to the side of the vacuum facility, and Figure 10 shows the updated EMPT v2.

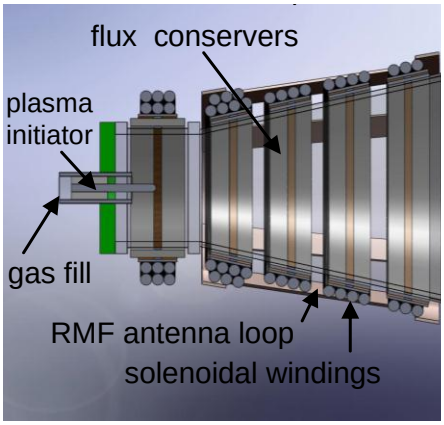

Figure 8. Cross Section of the EMPT with labeled components.

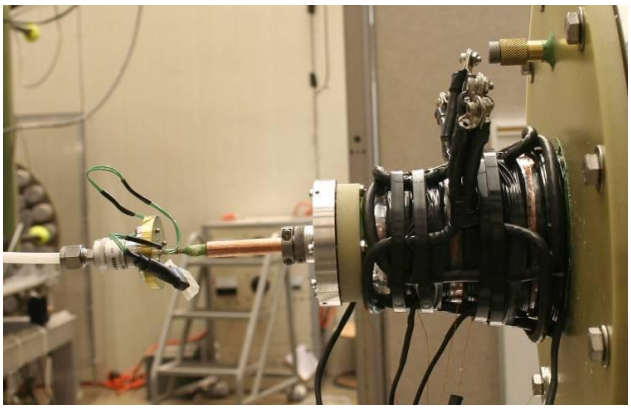

Figure 9. The EMPT v1 with bias field magnets, puff valve, pre-ionization discharge electrode and RMF antenna.

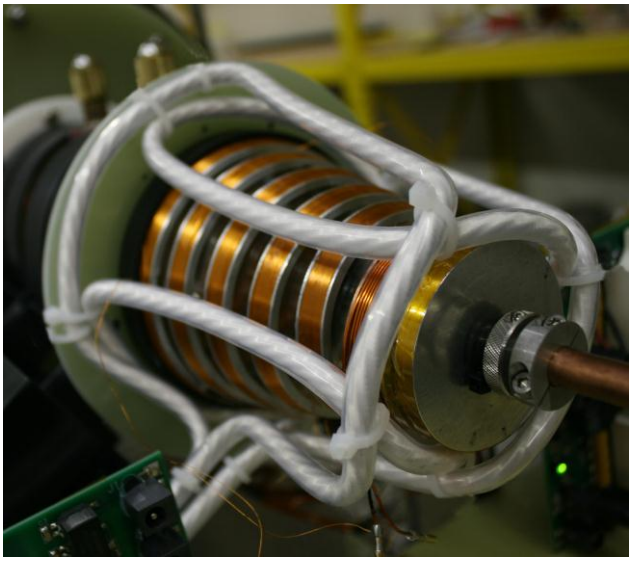

Figure 10. The EMPT v2 with upgraded RMF antenna, adjustable trim coil, and low-loss bias field coils.

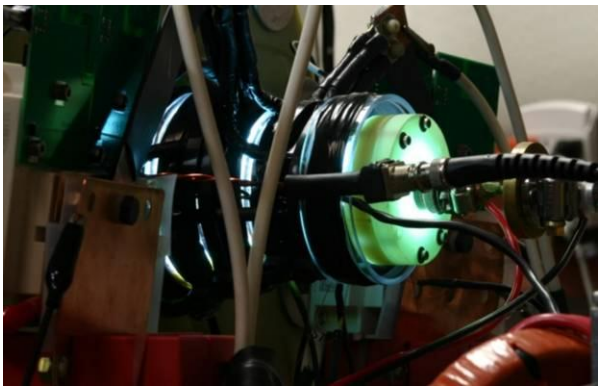

Figure 11. A long duration photograph of 20 Xenon FRC discharges in the EMPT.

SINGLE PULSE CHARACTERIZATION

The primary testing of the EMPT prototype used Xenon as the propellant, in order to fully optimize the thruster for deep space operation. Figure 12 shows the circuit loading for a typical Xenon discharge. It clearly shows that the EMPT begins full ionization within the first 2 oscillations. It then loads and energy is transferred quickly to the plasma. As the FRC forms and is ejected from the thruster the diamagnetic current drive allows for simple external investigation of the plasma. As shown in Figure 13 plasma is initiated in the small end of the discharge cone and progresses towards the exit during the discharge. It is seen that the FRC flux lifetime is quite short (as expected with this geometry) and the

thruster operates best when the FRC is ejected as soon as possible. The magnitude of magnetic field increase due to flux compression at the wall shows the temperature, density, and reversal of the plasma. Typical flux compression of >100% was seen in the EMPT for all discharge conditions, demonstrating complete ionization, reversal, radial contraction, and wall isolation of the plasmoid.

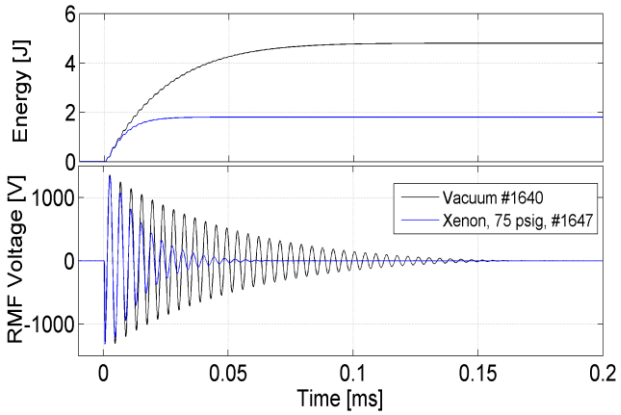

Figure 12. Time resolved plot of a typical Xenon FRC energy loading. Shown is the integrated energy deposited in the discharge coil for both vacuum and plasma discharges. The instantaneous capacitor voltage is show as energy is deposited in the plasma.

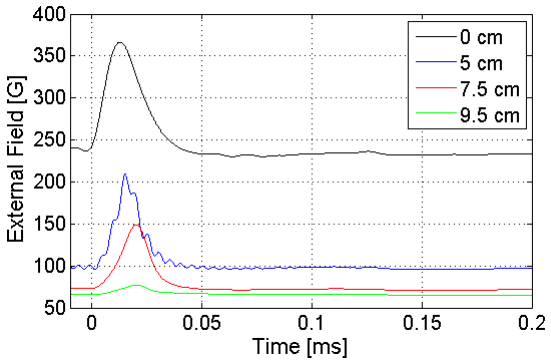

Figure 13. Time resolved external compressed field. Shown are both the slow bias field as well as the pulsed flux compression due to the formation and passage of the FRC.

Figure 13 shows the key data collected for the EMPT prototype. For each operating condition, two double probes were used to collect ion saturation current at two locations by comparing the arrival of the leading edge (red dot), peak (red), and mass-averaged (blue) time of arrivals an average and peak ion velocity can be found. Several key physical observations are seen in the downstream plasma density data. First, the FRC appears to be very well collimated, slight radial deviations from the approximate diameter of the thruster resulted in dramatic density falloffs. This can also be seen in the associated photographs. Additionally, velocities could easily reach greater than 20 km/s with Xenon. Figure 15 shows a photograph of the EMPT operated in the MSNW LLC facility in a multi-pulse operation with a slow camera.

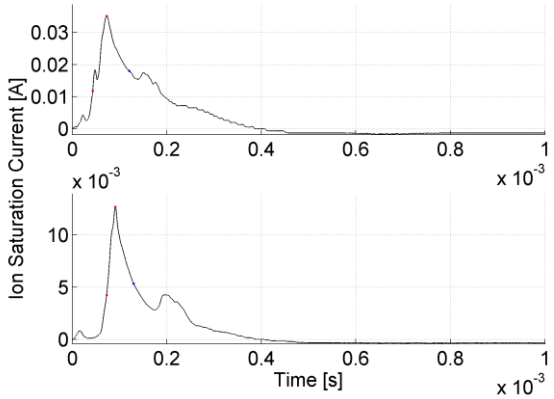

Figure 14. Normalized downstream plasma density for a translating FRC at two probe locations. Shown is a 2100 s Xenon FRC. Shot #1755.

Figure 15. Time averaged photograph of a 2 Joule Xenon EMPT discharge. Shown is burst mode operation inside of the MSNW LLC vacuum facility.

The EMPT is fundamentally a pulsed, RF device. It is completely driven by isolated fiber-optic trigger signals that require precise timing for optimal firing. The trigger units used have <20 ns of jitter for precision. A very slow (100+ ms) high energy density electrolytic capacitor is pulsed to provide a DC bias field. The propellant is puffed 1 ms before RMF initiation to provide enough seed flow. Pre-ionization begins approximately 25 μs before main RMF initiation. Figure 16 shows a typical loaded RMF discharge. Black is a vacuum discharge with no plasma and shows the DC coil resistance in the discharge circuit. Blue is the loaded, resistive plasma discharge. The RMF, high-Q capacitors have been charged and are discharged through the RMF antennas with the high-efficiency IGBT switches. The RLC circuit rings at the RMF frequency as describe earlier, generating the rotating field. Full ionization of the plasma is complete in 2-4 discharge cycles and the plasma is typically ejected within 20 μs. The RMF switches are allowed to fully drain the capacitor bank and then are opened and pulse charging continues.

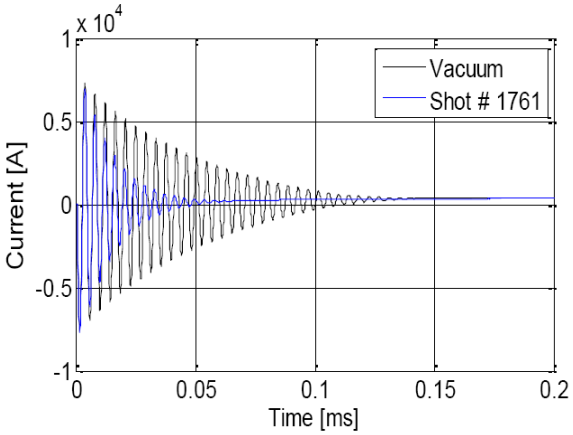

Figure 16. A typical loading and ringdown of the EMPT v1 prototype.

In the EMPT operating steadily, the thruster is operated differently from the prototype tested currently. As detailed later, it was found that for repetition rates greater than 1 kHz it was found that only a single, <50 microsecond pre-ionization discharge was necessary for steady state operation. The RMF discharge itself would then provide enough seed ionization for subsequent discharges.

More than 3000 discrete discharges were taken across a wide range of operating parameters. More than 20,000 FRCs were formed during multi-pulse operation. This wide testing range allowed for a complete picture of the operational parameter space of the EMPT on Xenon. It is important to note that these measurements are relatively preliminary and all utilize downstream plume diagnostics (Langmuir time of flight and ballistic pendulum) to garner thruster performance. Plume diagnostics are notoriously difficult to measure absolute performance parameters as background gas, chamber effects, and non-ideal plasma parameters have major effects on downstream characterization. Specific impulse in the following charts assumes full mass utilization, which is expected from previous FRC research and RMF physics as described earlier. The included error bars represent the expected error.

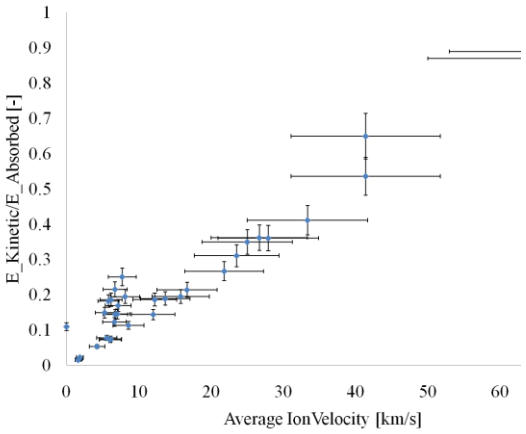

Figure 17. Scaling of Energy with ion velocity.

Figure 17 shows the compiled results of multiple operating conditions, including bias field and neutral fill. It shows the general trend of thruster efficiency, or literally, the directed kinetic energy divided by the energy coupled to the plasma. PPU and circuit loss energy is not included in this analysis. These data show a clear trend, in that ionization energy (eV/ion) is relatively constant and overall efficiency increases with plasma velocity. It is believed that with further optimization and circuit improvements the lost energy can be reduced even further. These data use both the ballistic pendulum and TOF Langmuir probes to determine velocity.

Figure 18 and Figure 19 show the directed kinetic energy, total absorbed energy, average ion velocity, and average thrust impulse, respectively as a function of ‘puff time’. The ‘puff time’ is the time between the initiation of the 400-600 microsecond neutral gas puff and the initiation of the RMF discharge. In general this time correlates with increases neutral density within the discharge chamber and the plasma density of the FRC. Several distinct trends can easily be seen. All discharges show the same general trend. Decreasing neutral gas in the discharge cone decreases the mass of the plasmoid and dramatically increases the exit velocity of the ejected plasmoid. Additionally, as the mass of the plasmoid decreases the total thrust impulse decreases. There does appear to be an optimal region, where kinetic energy is maximized as both impulse and velocity increase. As neutral gas is decreased further (greater than -1 ms), the RMF no longer has sufficient electrons to drive the large diamagnetic currents and fails to eject a coherent FRC. This is consistent with basic RMF theory and was measured for all gases tested, though the final optimal specific impulse and efficiency were heavily dependent on molecular mass. At the higher density end of the scale (puff times less than -2 ms) the RMF has a sufficient supply of background plasma and current and can both load efficiently and drive a very large diamagnetic current. However, the FRC plasmoid mass is large and while a coherent, reversed FRC is ejected, it is ejected at low velocities and consequently lower total efficiencies. Perhaps most interesting, the overall energy loss per ion in the plasmoid appears to be constant. Further work must be done in fully measuring the total ion content of a

plasmoid in order to accurately determine energy loss per ion. As expected, increasing available RMF energy increased both thrust and velocity for a given background pressure. Higher pressures were able to be fully ionized and accelerated to high velocity, while low pressures were relatively unchanged. It is unknown as to the upper limit on EMPT power density, for the testing equipment used, the EMPT thruster thrust, velocity, and efficiency continued to increase with increasing per-pulse energy.

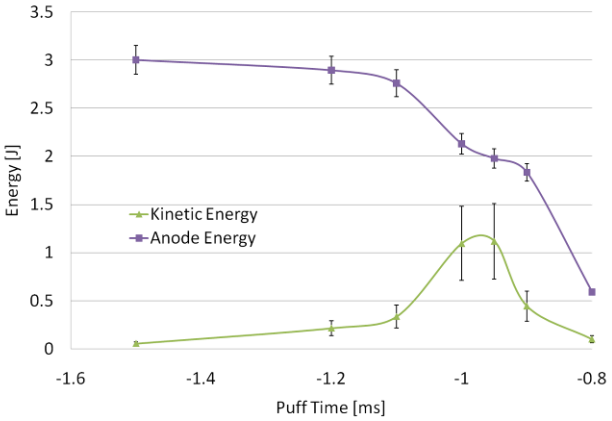

Figure 18. Measured kinetic energy and absorbed energy for a 75 psig Xenon plasmoid. Shot #1640-1725.

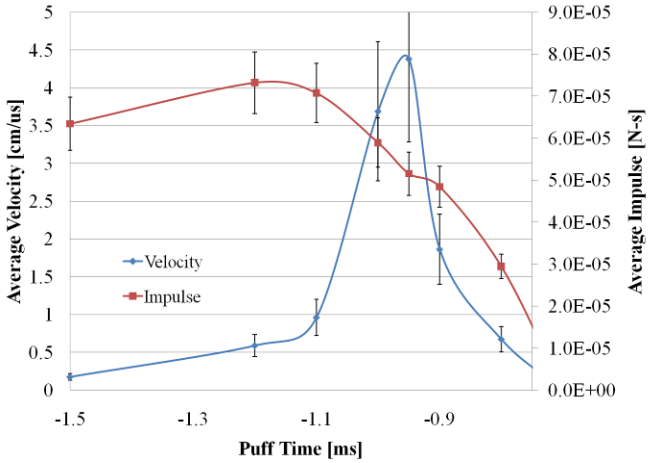

Figure 19. Measured thrust impulse and downstream plasmoid velocity for a 75 psig, 1300 V, Xenon plasmoid. Shot #1640-1725.

MULTI-PULSE CHARACTERIZATION

As described earlier, a multi-pulse, pulse charge circuit was designed and implemented on the EMPT. In these tests, a 2 mF backing capacitor was used rather than a steady power supply. For the multi-pulse operation, the EMPT was tested from 1-50 discharges and multiple puff durations. Figure 20 shows the capacitor voltage for a vacuum and plasma discharges for the EMPT operating at 2800 Hz. The first discharge shown is a 250 Voltage discharge due to initiation of the pulse charging, while subsequent discharges are 1300 Volts. The decrease in peak voltage is due to the depletion of energy in the pulse-charge electrolytic backing capacitors. To the limit of the author's knowledge, this multi-pulse operation is a first for any pulsed inductive thruster. It was critical in these tests to establish a steady gas flow through the device for multi-pulse testing. This was verified with the typical fast ion gauge measurements described in previous work [9].

Figure 21 shows the downstream double probe ion saturation current as a function of time. It clearly shows that multiple, high density plasmoids are being ejected from the EMPT and traveling at high speed. Changes in downstream ion density and velocity are due to both the decrease in energy in the EMPT discharge, downstream neutral gas, and initial stabilization of the gas flow through the puff valve. As the gas puff length is increased, the RMF energy is better coupled and multiple discharges form and are ejected. Additionally, the leading and trailing edge of the gas flow leads to clear non-optimal discharge conditions within the thruster. Figure 22 shows the EMPT operation for increasing gas flow. It is important to note that this is for the exact same discharge conditions, as the electronics within the EMPT can be operated independently of neutral flow, a unique advantage of pulsed inductive thruster

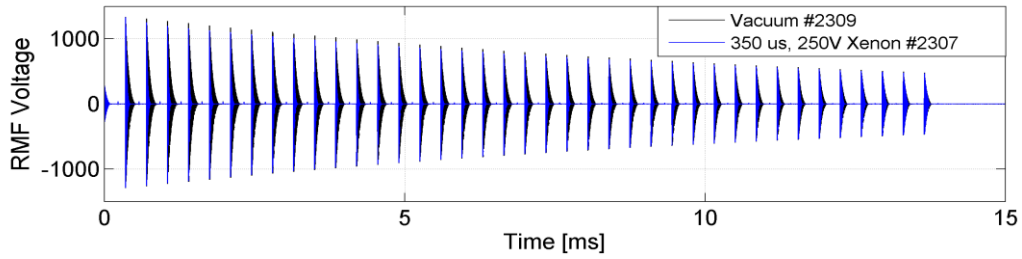

Figure 20. Vacuum and plasma capacitor voltages for 40 discharges at 2800 Hz discharge frequency.

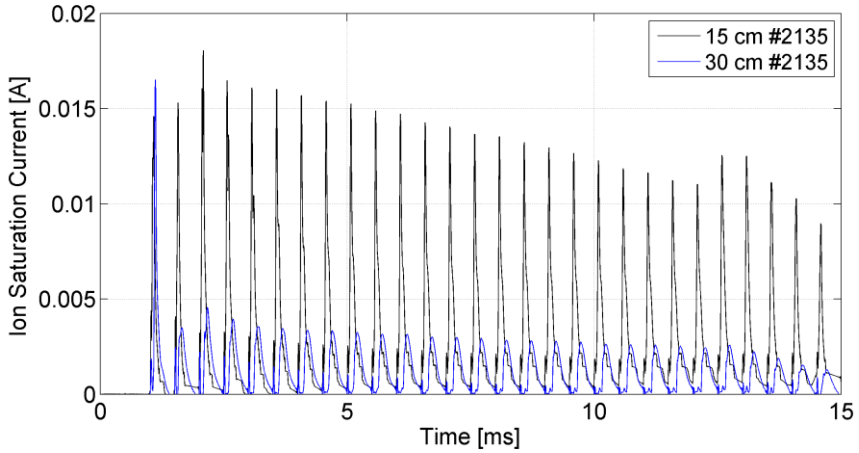

Figure 21. Downstream double probe current at two locations for high-speed multi-pulse operation.

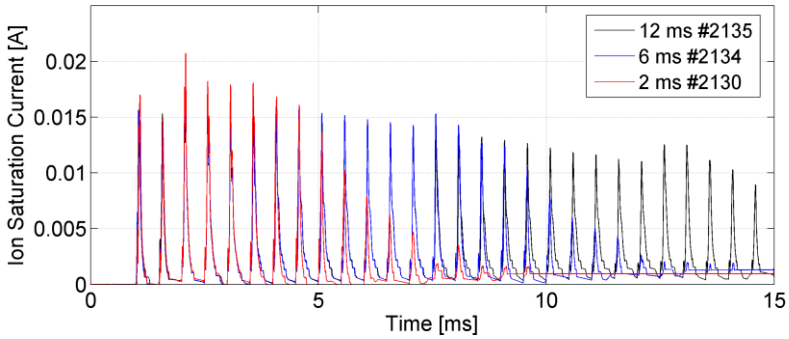

Figure 22. Downstream double probe current at a single axial position, 15 cm downstream for high-speed multi-pulse operation. Shown are 40 electrical discharges for increase gas puff lengths. The 12 ms puff is essentially steady state.

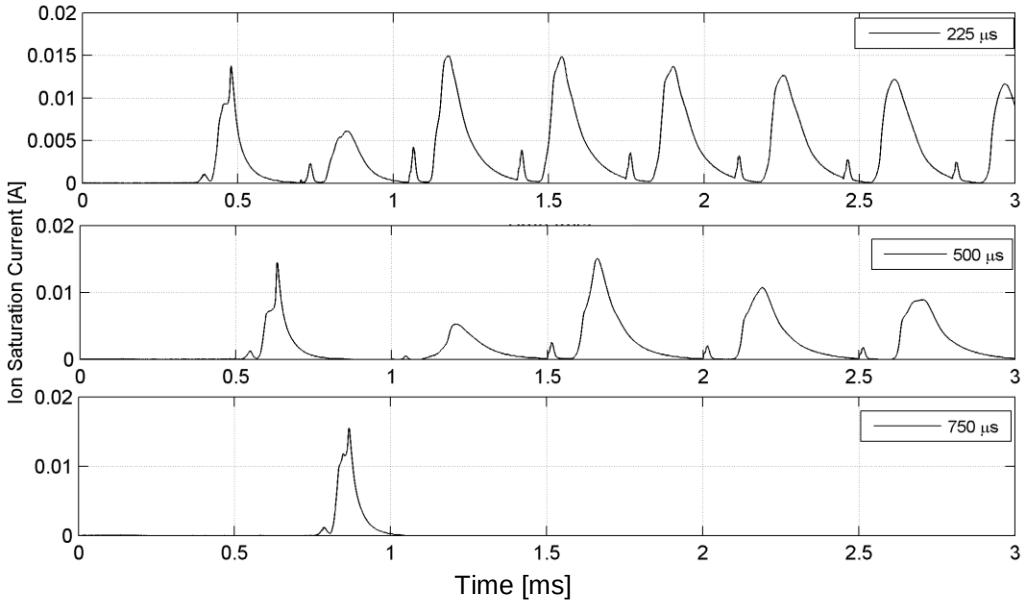

Figure 23. Downstream double probe current for various discharge spacing. Shown are shot #2328, 2386, and 2447.

Finally, one of the key discoveries in the operation of the EMPT that has redefined the steady state operation of the thruster is the effect of a transient pre-ionization on the long term operation of multiple discharges. It was found that a single, 20 microsecond pre-ionization discharge was sufficient for multiple, indeed unlimited, RMF discharges if the spacing between discharges was less than 500 microseconds. It was found that the seed ionization provided by the full energy RMF discharge was sufficient to allow for subsequent discharges with similar loading, plasma formation, diamagnetic, and downstream plasma properties. For discharges less than 2 kHz, discharges were erratic and in some cases non-functional beyond 2-5 discharges and is shown in Figure 23**.** For every discharge condition tested, the first and second FRCs formed were not like the later discharges. This can simply be interpreted as the initiation of the residual ionization required to start the FRC discharges took several complete discharges to become sufficiently large in magnitude and dispersion.

Perhaps most interesting, both thrust and energy increase as the number of FRCs are added to the discharge, and appears to do so in the expected manner. Figure 22 shows a 6 ms gas puff with increasing number of electrical discharges. As expected, increasing the number of FRC discharges dramatically increases both the energy absorbed by the

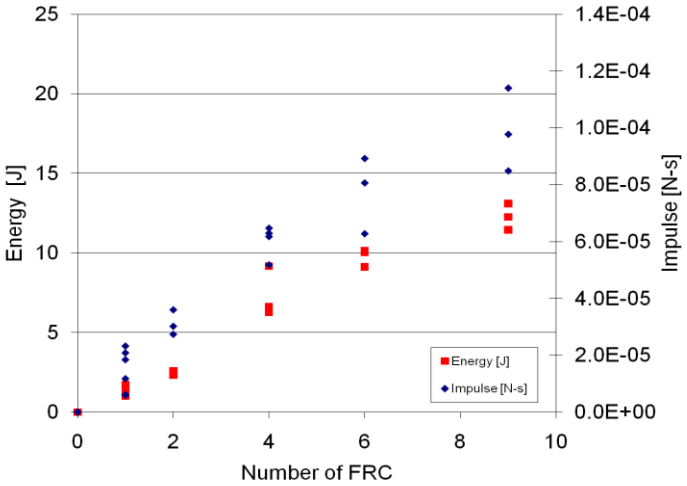

Figure 24. The energy and thrust impulse for multiple ejected plasmoids. Shown is a 6 ms gas puff with increasing number of electrical discharges at 2 kHz.

plasma as well as the total impulse. There is influence from multiple high-density plasmoids impinging with the ballistic pendulum that will lead to erroneous decreases in measured impulse, however, it is clear that the thruster is producing increased thrust and performance as the operational period is extended.

THERMAL TESTING

Experimental Testing

A complete set of thermal testing and modeling was conducted for the 1 kW EMPT. These tests seek to explore and ultimately engineer solutions for the steady operation of a high intensity pulsed discharge. The experimental set up was conducted both in and out of vacuum, however the primary tests to be described here were done out of vacuum. The thruster set up was arranged such that the pulse inducting charging system and pulse energy storage and switching were all used as in the thruster tests described in the previous sections. Testing was conducted with and without a simulated plasma load. This simulated plasma was 0.5 mm thick stainless steel sheet braised into a conical and water tight shell. One unique advantage of inductively driven thrusters is that a highly accurate equivalent plasma load can be inserted in the thruster without electrical connections as energy couples purely inductively. For these simulations, the circuit Q (or in the case, equivalent plasma resistance) was used as the metric in designing the equivalent plasma load. This was done so that the same energy dissipated in the plasma in the multi-pulse characterization tests was also dissipated into the simulated load for these thermal tests. Two distinct circuits were tested. First, the same monolithic high-power IGBT that was used in the aforementioned multi-pulse characterization section was tested. Secondly, a highly distributed array of low-power IXYS IGBTs were tested. For each circuit a similar pulsed inductive charging and capacitive systems was used

Numerous thermal sensors were used to determine component temperatures during the thrusters simulated steady state operations (up to 4 hrs and 43 million discharges). The circuit wave form for the monolithic IGBT as tested is shown in Figure 7. There were ten specific geometric points that were measured for thermal increase. The RMF antennas were measured along their entire length at several locations and averaged. The pulse charging inductor was measured at its surface. The aluminum heat sinks of the IGBT switches were measured at two points. The pulse charging diode was measured at its heat sink and the strip line transition between RMF antenna and IGBT switch was measured at the interface junction itself.

Figure 25 and Figure 26 show the rise in temperature as a function of discharge for the various subcomponents as described above. As can be seen it is clear where the majority of the heating occurs as well where it must be mitigated. Somewhat surprisingly there was only minor heating in the RMF antennas and capacitors, while the majority of the heating occurred at the interconnects and switches. This shows just how crucial connections, whether they be mechanical, soldered, braised or welded, are to total circuit resistances. Known circuit resistances account for approximately half of the total circuit resistance, which suggests that the remaining half lies in the semi-conductor switches. This is verified by the thermal data taken here. Fortuitously the easiest components to heat sink are these semiconductor switches. These tests clearly show that highly distributed switching is important for thermal and heat management. Additionally, these tests showed that there is little concern about PPU heating in either air or vacuum environments at this power level.

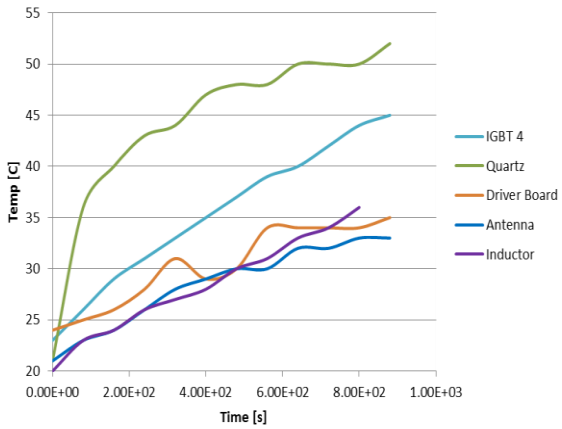

Figure 25. Thermal testing of monolithic IGBT switches. Shown are temperatures [C] for various circuit components and RMF antenna Load. Total power was 1 kW into 2 switches.

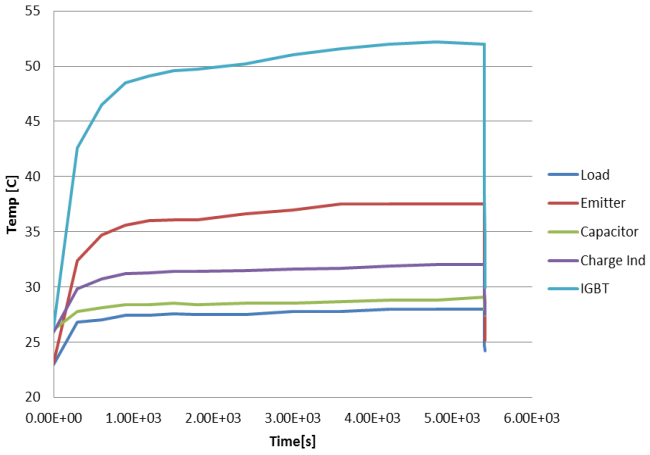

Figure 26. Steady thermal operation for 1.5 hrs. Shown are temperatures [C] for various circuit components and RMF antenna Load. Total power was 1 kW into 24 distributed switches.

Steady Thermal Modeling

A range of ANSYS thermal models were implemented in order to investigate the steady thermal conditions of the EMPT. These models initially used highly transient thermal loading in a simple quartz cylinder, as well as antenna and switch conductors. ANSYS MultiPhysics v12 transient and steady thermal models were used. Initial testing showed that the highly transient nature of the EMPT leads to challenging computational requirements. Therefore initial testing was done for both a highly-temporally resolved transient solution as well as a steady solution to a simplified quartz geometry. Both long-term and instantaneous solutions converged on each other as shown in Figure 28. These simulations showed quite clearly that it is possible to simulate a fully transient loading with a steady operating thruster. It was found that the while the conductors and insulators have an instantaneous heat load on a particular surface the thermal diffusion times of the materials, particularly the ceramic insulators was so long that any transient heat load was damped out over the long timeframe. Additionally, since the thruster duty cycle was so low (<15%), the primary radiated power loss was due to the average heat loads in the thruster. In Figure 27 a 50 microsecond, 15 kW heat load was applied to the inner quartz cylinder at a 3 kHz repetition rate with a temporal resolution of 10 μs, while in Figure 28 a steady 1 kW load was applied.

Therefore with high confidence a detailed model was assembled to investigate average temperature as a function of the final thruster, geometry, materials, and individual component energy and thermal loading. Shown in Figure 27 through Figure 30, several thermal loads were simulated using various heat sinks, applied load magnitudes, and thruster operating conditions.

The heat loads simulated in the Figure 27 through Figure 30 were as follows:

- Electronics backplane – 100 W (measured)
- Quartz inner insulator – 50 W (rough estimate)
- RMF antenna – 13 W each (measured)
- Flux conserver – 8 W each (calculated from measured parameters)
- Cooled baseplate – 295 K fixed

Note: This has an overall input efficiency of 75%, with the remaining efficiency loss within the thruster dedicated towards frozen flow and plasma losses. These data are considered a worst case scenario.

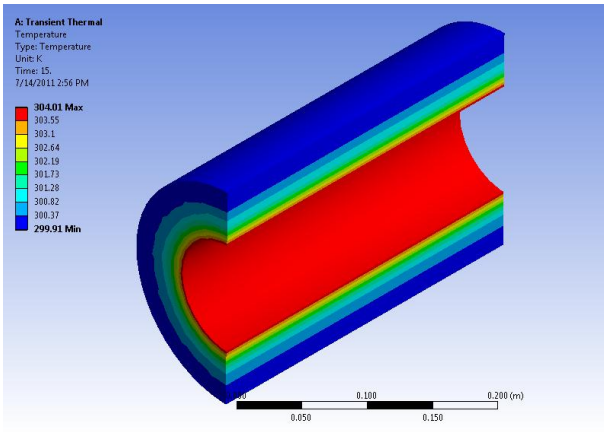

Figure 27. Full, transient thermal model of a quartz cylinder. A 50 microsecond heat load is pulsed at 3 kHz. Simulation run time was approximately 36 hrs.

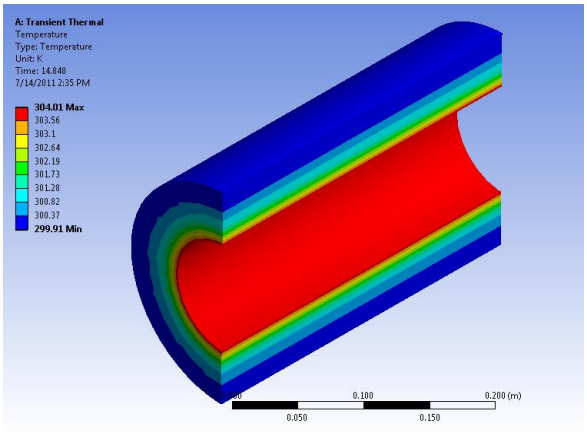

Figure 28. Steady thermal model with an 1kW average heat load to the surface. All surfaces were radiation with an emissivity 0.93 (quartz). Simulation run time was 3 minutes**.**

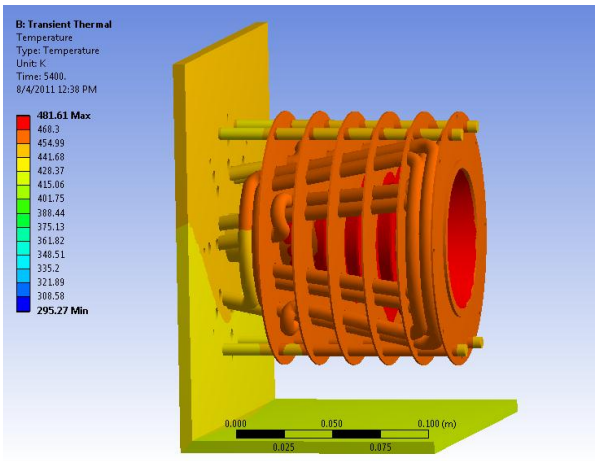

Figure 29. Thermal model with complete expected heat loads and no heat sinks. Temperature shown is in Kelvin.

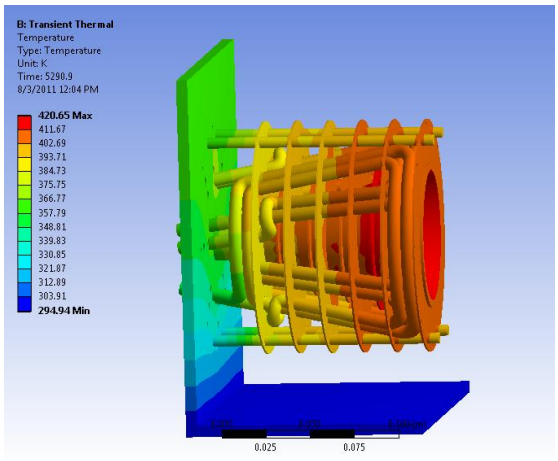

Figure 30. Thermal model with complete expected heat loads and a cooled baseplate. Temperature shown is in Kelvin.

From these simulations, several key parameters can be determined. First, it took approximately 1.5 hrs for the thruster to reach equilibrium temperature. Secondly, the thruster temperatures are well within the range for the materials chosen. These temperatures were not surprisingly higher for the non-heat sunk case, but still within a reasonable range. Additionally, operating temperatures in a vacuum are significantly higher than for the air case, particularly for the thermal loads described above. The addition of secondary radiating surfaces (the flux conservers) allowed significant decrease in the final operating temperature of the thruster body, particularly the antenna.

DESIGN MITIGATION AND CONCERNS

Thorough modeling and experimental effort has begun in order to investigate the realities of thermal loading in a steady operating electromagnetic thruster. From this it is also clear that there are concerns for switch and wall loading, as they are a majority of the input radiant heat given the thruster design and characteristics of the EMPT. Therefore, in any high current pulse device, very particular design consideration must be taken for the following components with the author's view of critical issues and required solutions.

Antenna and High Current Coil: Resistance in this component is easily mitigated through either the use of advanced Litz wires or a sufficient amount of copper. This component is critical and must be considered throughout the design effort. In the system as designed thermal concerns are negligible due to the high specific conductivity of the Litz wire.

Insulator Material: As with all plasma based systems, the thruster insulator and thruster walls bears the brunt of high energy plasma deposition. However, in pulse inductive thruster, and particularly FRC-based ones, the wall is shielded due to the low thermal diffusion rates across the magnetic vacuum boundary. Therefore, during the highest energy and highest velocity segments of the discharge, there is expected to be zero thermal loading from the wall. However, during initial plasma formation and pre-ionization, this wall loading may not be negligible. In experiments to date there has been no major thermal loading to the wall detected. This will be continually monitored and further confirmed in later experiments.

Switch Electronics: In the design as presented, switch electronics form the major loss resistive loss mechanism, as well as the major thermal loading concern. This is ideal as these are the components that can be most easily regulated, as well as the components that are the simplest to distribute. In order to mitigate heat concerns, these switches must be highly parallelized, distributed away from the thruster insulator, and be radiatively shielded from thruster and antenna thermal loads. This paper has described two experimental conditions in which single, monolithic switches are used as well as distributed switching and shows the dramatic decrease in thermal and lifetime concerns with distributed electronics.

Capacitors: In the design tested, thermal loading to the capacitors is negligible. However, capacitors are a highly sensitive component and particularly at higher energies difficult to heat sink. Therefore, for both resistance, inductive and thermal issues, it will always be preferable to design distributed capacitors in which the heat is easily removable, as well as only using the highest=Q capacitor dielectric materials for both circuit efficiency and thermal deposition. The authors of this paper believe that ceramic capacitors will be required for all space-rateable and steady operating thrusters.

Ancillary and Charging Electronics: In the design presented here was minor heating and resistive losses in the ancillary electronics. The only concern is adequate thermal shielding from the switches and insulator. Future designs will even further distribute and parallelize electronics antenna components, as well as investigating higher temperature insulator and materials.

SUMMARY

A steady operation FRC thruster has been demonstrated at MSNW, a milestone in the pulsed inductive propulsion community. This thruster has shown that, ultra-low, 0.5-2 Joule FRCs can be formed in Xenon. This paper presented initial results from the first steady operation of a pulsed FRC thruster with up to 50 FRC plasma discharges demonstrated in the laboratory. Steady operation of the PPU and a simulated load were demonstrated with 4 hours of operation and more than 47 million discharges. Several key conclusions can be shown from this work. First, the gas utilization in an FRC thruster appears to be quite high and as long as the thruster is operated in a burst mode with multiple plasma discharges per gas puff or for steady flowing gas. Secondly, the first three discharges of a pulsed electromagnetic thruster are not indicative of the later and steady operating thruster performance. And while scaling and overall thruster operation can be determined from single-pulse operation, multi-pulse and steady operation of the thruster is required for complete performance determination.

A steady-operating, lightweight pulse charging system has been demonstrated with both a simulated and Xenon plasma load. This system has the capability to directly draw from a low voltage battery and pulse inductively charge the thruster operating capacitors to the required voltages in a single switch operation. This technique has been shown to be highly efficient over a wide operational range. And finally, a detailed thermal model has been constructed to investigate the steady operation of a pulsed thruster. Currently ongoing work and future publications will focus on the steady operating performance of a 1 kW FRC thruster.

ACKNOWLEDGEMENTS

The authors would like to thank NASA for support of this effort.

REFERENCES

1. A. Savtchkov, K. H. Finken, and G. Mank, “Development of a fast valve for mitigating disruptions in tokamaks”. Review of Scientific Instruments, V 73, N 10 (2002).

2.María M. Milanese, Jorge O. Pouzo, Osvaldo D. Cortázar, Roberto L. Moroso " Fast valve and nozzle for gas-puff operation of dense plasma focus", Review of Scientific Instruments (AIP), Vol. 77, no. 3 (2006).

3. Kirtley, D., Slough, J., and Pihl, C. “Pulsed Plasmoid Propulsion: Air-Breathing Electromagnetic Propulsion”. International Electric Propulsion, IEPC-2011-015 (2009).

4. A.L. Hoffman, H.Y. Guo, K.E. Miller, R.D. Milroy, “Long Pulse FRC Sustainment with Enhanced Edge Driven Rotating Magnetic Field Current Drive”, Nucl. Fusion 45, 176 (2005).

5. Polzin, K.A., "Scaling and systems considerations in pulsed inductive plasma thrusters," IEEE - Transactionson Plasma Science, Vol. 36, No. 5, 2008, pp. 2189-219.

6. Ziemer, J.K. “Performance Scaling of Gas-Fed Pulsed Plasma Thrusters” Doctoral Thesis, Princeton University, 2001.

7. H.A. Blevin and P.C. Thonemann, “Plasma Confinement using an Alternating Magnetic Field”, Nucl. Fus. Suppl. Part I, 55 (1962).

8. Francis F. Chen, “Physics of helicon discharges”, Phys. Plasmas 3, 1783 (1996).

9. Slough, J., Kirtley, D. E., Weber, T., “Pulsed Plasmoid Propulsion: The ELF Thruster,” IEPC-2009-265, 2009.

10. Kirtley, D. E., Slough, J., Weber, T. E., “Pulsed Plasmoid Propulsion: The ELF Thruster,” Joint Army Navy NASA Air force meeting, Colorado Springs, CO., 2010.